An Electrochemical Model for Prediction of Corrosion of Mild Steel in Aqueous Carbon Dioxide Solutions

S. Nesic, J. Postlethwaite,** and S. Olsen****

ABSTRACT

A predictive model was developed for uniform carbon dioxide (CO_2) corrosion, based on modeling of individual electrochemical reactions in a water-CO_2 system. The model takes into account the electrochemical reactions of hydrogen ion (H^+) reduction, carbonic acid (H_2CO_3) reduction, direct water reduction, oxygen reduction, and anodic dissolution of iron. The required electrochemical parameters (e.g., exchange current densities and Tafel slopes) for different reactions were determined from experiments conducted in glass cells. The corrosion process was monitored using polarization resistance, potentiodynamic sweep, electrochemical impedance, and weight-loss measurements. The model was calibrated for two mild steels over a range of parameters: temperature (t) = 20°C to 80°C, pH = 3 to 6, partial pressure of CO_2 (P_{CO_2}) = 0 bar to 1 bar (0 kPa to 100 kPa), and ω = 0 rpm to 5,000 rpm (v_p = 0 m/s to 2.5 m/s). The model was applicable for uniform corrosion with no protective films present. Performance of the model was validated by comparing predictions to results from independent loop experiments. Predictions also were compared to those of other CO_2 corrosion prediction models. Compared to the previous largely empirical models, the model gave a clearer picture of the corrosion mechanisms by considering the effects of pH, temperature, and solution flow rate on the participating anodic and cathodic reactions.

KEY WORDS: aqueous solutions, carbon dioxide corrosion, carbon steel, films and film formation, flow, mass transfer, modeling, pH, temperature, uniform corrosion, weight loss

INTRODUCTION

Most of the models used in industry to predict carbon dioxide (CO_2) corrosion rates are "worse case" models. The ones in the public domain, such as the models of deWaard and Lotz[1] and Dugstad, et al.,[2] are semiempirical. Such models do not lend themselves to extrapolation easily. Moreover, including the effects of new parameters is possible only through correction factors that further obscure the underlying corrosion mechanisms and that can have dubious interactions once more than one correction factor is applied.[1] Because of the high cost and long duration of corrosion experiments, development of improved prediction models is required.

As part of a long-term project on CO_2 corrosion conducted in Norway, a fully theoretical approach has been taken by modeling individual electrochemical reactions occurring in a water-CO_2 system. This is not a novel approach per se in that such models have been created for advanced analysis of polarization scans[3-8] and for educational purposes.[9] In the area of CO_2 corrosion, Bonis and Crolet briefly mentioned one such model, but they have not presented it in detail.[10] They demonstrated performance of the model by comparing it to predictions made with the model of deWaard and Milliams, obtaining results of a similar order of magnitude.[11] Gray, et al., presented an electrochemical model as part of an experimental

Submitted for publication December 1994; in revised form, July 1995.

* Institutt for Energiteknikk, P.O. Box 40, N-2007, Kjeller, Norway. Present address: Department of Mechanical Engineering, University of Queensland, Brisbane, Qld. 4072, Australia.
** University of Saskatchewan, Saskatoon, Canada. Present address: Institutt for Energiteknikk, P.O. Box 40, N-2007, Kjeller, Norway.
*** Statoil, Postuttak, 7004, Trondheim, Norway.

0010-9312/96/000067/$5.00+$0.50/0
© 1996, NACE International

study of CO_2 mechanisms.[12-13] That study was extended over too broad a pH range, so that all stated assumptions did not hold (especially for pH > 7, where protective films probably formed). However, the overall theoretical approach served as an inspiration for the present work.

Processes to be modeled in a water-CO_2 system are the electrochemical reactions at the metal surface and the transport processes of all the species in the system, such as hydrogen ions (H^+), CO_2, carbonic acid (H_2CO_3), and iron (Fe^{2+}). The present work focuses on the model of the electrochemical reactions occurring in an acidic solution with dissolved CO_2. Transport processes were treated in a simplified way by assuming independent diffusion of the species and by using well-established mass-transfer coefficients for the hydrodynamic systems of interest: the rotating cylinder and pipe flow. A more detailed approach to the coupled transport of species in a water-CO_2 system will be incorporated in the future.[14]

Performance of the model was demonstrated by comparing predictions to results from flow loop experiments and results of the CO_2 corrosion prediction models of deWaard and Lotz[1] and Dugstad, et al.[2]

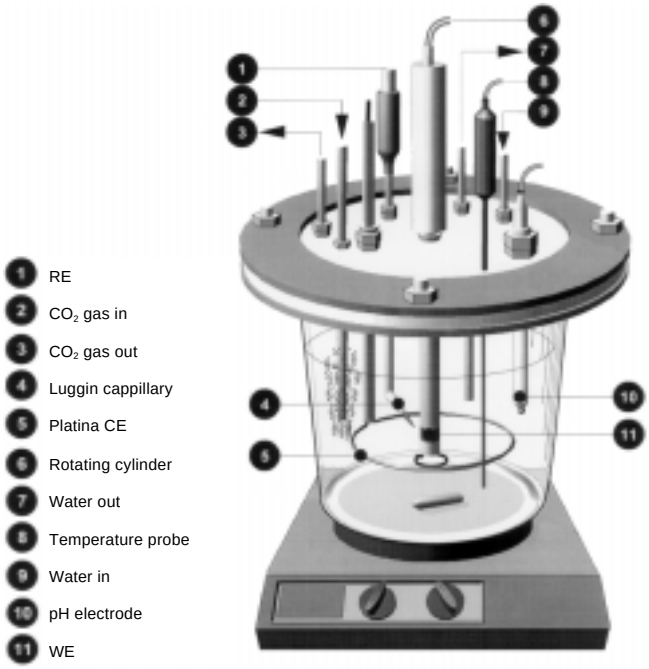

FIGURE 1. *Schematic of the experimental cell.*

EXPERIMENTAL

Equipment

Experiments were conducted at atmospheric pressure in a battery of eight glass cells. Gas (CO_2 or nitrogen [N_2]) was bubbled through the cells continuously. The corrosion process was studied using electrochemical techniques and occasionally checked using weight-loss measurements. A three-electrode setup was used (Figure 1). A rotating cylinder electrode (RCE) with a speed control unit (0 rpm to 5,000 rpm)[(1)] was used as the working electrode (WE). A concentric platinum ring was used as a counter electrode (CE). A saturated silver-silver chloride (Ag-AgCl) reference electrode (RE) was connected to the cell externally via a Luggin capillary and a porous wooden plug. The rotation speed of the WE was controlled using a stroboscope. The pH was monitored with an electrode immersed in the electrolyte. Temperature (t) was followed with a platinum-100 probe that also served as an input for the temperature regulating system, which was a hot plate combined with a magnetic stirrer. Oxygen concentration was monitored using an Orbisphere† oxygen meter. The concentration of Fe^{2+} was measured occasionally using a photospectrometric method. The concentration of CO_2 in the water also was measured in selected experiments. Electrochemical measurements were made using a Gamry Instruments† potentiostat with an eight-channel multiplexer connected to a personal computer.

Material

Two low-carbon steels were tested: St52 (corresponding to ASTM A537 Grade 1, [UNS K12437])[(2)] which is a typical construction steel and X-65 steel, which is a typical pipeline steel. Chemical compositions of the steels are given in Table 1. The WE was machined from the parent material into a cylinder 10 mm (0.394 in.) in diameter and 10 mm (0.394 in.) in length. The exposed area of the specimen was 3.14 cm^2 (0.487 $in.^2$).

Procedure

The glass cells were filled with 3 L (0.793 gal) of electrolyte, which was distilled water + 1 mass% sodium chloride (NaCl). In different experiments, CO_2 or N_2 was bubbled through the electrolyte (min. 60 min) to saturate or deaerate the solution. Monitoring of pH and O_2 concentration was used to judge when the solution was in equilibrium. When needed, hydrochloric acid (HCl) or sodium bicarbonate ($NaHCO_3$) was added to adjust the pH. The temperature was maintained within ± 1°C in all experiments.

Before each polarization experiment, the steel WE surface was polished using 500- and 1,000-grit silicon carbide (SiC) paper, washed with alcohol, mounted on the specimen holders, and immersed into the electrolyte. The free corrosion potential was

(1) 5,000 rpm for the cylinder corresponded to a peripheral velocity of 2.61 m/s (0.8 ft/s), a shear stress of 25 Pa, and a Reynolds number of 26,175.

(2) UNS numbers are listed in *Metals and Alloys in the Unified Numbering System*, published by the Society of Automotive Engineers (SAE) and cosponsored by ASTM.

† Trade name.

TABLE 1
Chemical Composition of the Steels Used for the WE (mass%)

	C	Mn	Si	P	S	Cr	Cu	Ni	Mo	Al
X-65	0.065	1.54	0.25	0.013	0.001	0.05	0.04	0.04	0.007	0.041
St52	0.130	1.25	0.35	0.022	0.004	0.12	0.31	0.08	0.02	0.035

TABLE 2
Experimental Conditions

Test solution	Water + 1 mass% NaCl
Test material	Low-carbon steel, St52 and X-65
Temperature	20°C to 80°C
Pressure	1 bar N_2 or CO_2
pH	3 to 6
Fe^{2+}	< 1 ppm
Dissolved oxygen	< 20 ppb
Velocity	Static to 5,000 rpm
Test duration	0.5 h to 48 h
Sweep rate	0.1 mV/s to 0.2 mV/s
Polarization resistance	From –5 mV to 5 mV (vs E_{oc})
AC impedance	± 5 mV vs E_{oc} from 1 mHz to 100 kHz
Potentiodynamic sweep	From –600 mV to 200 mV (vs E_{oc})
IR compensation	Automatic or manual

followed immediately after immersion. Depending on the conditions, the potential stabilized within ± 1 mV in 1 min to 10 min.

Polarization resistance (R_p) measurements were conducted by polarizing the WE ± 5 mV from the free corrosion potential and scanning at 0.1 mV/s. In most experiments, automatic IR drop compensation was used. In other cases, solution resistance was measured independently using alternating current (AC) impedance, and the measured R_p then was corrected. AC impedance measurements were done by applying an oscillating potential ± 5 mV around the free corrosion potential to the WE using the frequency range 1 mHz to 100 kHz.

At the end of each experiment, the potentiodynamic sweeps were conducted, starting 500 mV to 600 mV below and finishing 100 mV to 200 mV over the free corrosion potential. The typical scanning rate was 0.1 mV/s to 0.2 mV/s. In some cases, the cathodic and anodic sweeps were conducted separately starting from the free corrosion potential. The cathodic sweeps sometimes were repeated by sweeping in the opposite direction, without significant difference in the result. In each experiment, the anodic sweeps were conducted only once for a single WE specimen and a given electrolyte (starting from the free corrosion potential) since they altered the specimen surface and contaminated the electrolyte with significant amounts of dissolved iron (Fe^{2+} > 3 ppm). Typically, the Fe^{2+} concentration was kept at < 1 ppm.

[3] Current is shown throughout this work in A/m^2. This is convenient as for iron dissolution: 1 mm/y = 1.155 A/m^2.

Potentiostatic measurements also were conducted in which the potential was kept at a desired level while the rotational speed was varied. Experimental conditions are summarized in Table 2.

RESULTS AND DISCUSSION

More than 50 glass cell experiments were conducted. Many experiments were repeated several times to check reproducibility of the results. To clarify the effect of CO_2, some experiments were done in solutions purged with N_2 where the pH was adjusted by adding HCl. Selected experiments have been presented here to explain the most important effects.

Effect of CO_2

Measurements at pH 4 — In Figure 2, potentiodynamic sweeps done on St52 steel are compared for two solutions at pH 4, first for one purged with N_2 (pH adjusted by adding HCl) and the other for one purged with CO_2 (pH adjusted with $NaHCO_3$).[3] Experimental results are overlaid with the predictions of individual reactions generated with the model presented. The solution containing CO_2 produced higher cathodic currents, probably because of the additional cathodic reaction in the direct reduction of H_2CO_3.[11]

This was investigated using potentiostatic measurements where the potential was kept in the limiting current (i_{lim}) region while the rotation speed was varied (Figure 3). The gap between the two curves even at stagnant conditions confirmed the assumption of Schmitt and Rothman[15] and Eriksrud and Søntvedt[16] that there is a flow-independent component of i_{lim} in CO_2 solutions that probably is controlled by a chemical step (i.e., the hydration of CO_2 to H_2CO_3). However, the present work concerned the turbulent region comprising all the points above ω > 50 rpm. In this region, a linear relationship was observed for i_{lim} vs $\omega^{0.7}$ in both CO_2 and HCl solutions, which was to be expected from theory.[19] At a given flow rate, i_{lim} for a CO_2 solution tentatively can be separated into three components: one relating to the diffusion of H^+, one to the hydration of CO_2, and one to the diffusion of H_2CO_3 respectively; in agreement with the proposals of Schmitt and Rothman.[15]

Figure 2 shows that the H_2O reduction was under charge-transfer control and did not seem to be affected significantly by addition of CO_2. The same was true for the anodic dissolution of Fe^{2+}. The Tafel

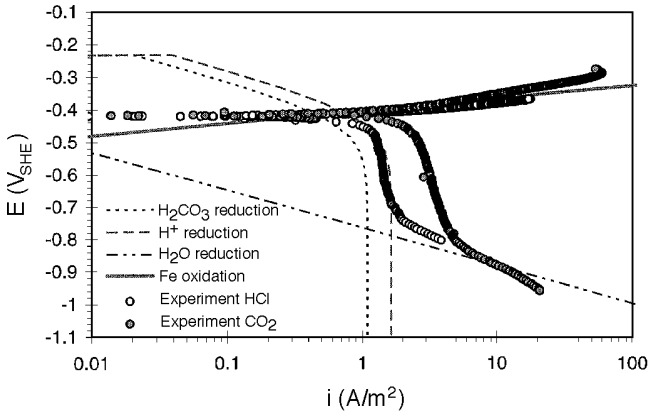

FIGURE 2. *CO_2 effect at pH 4, water + 3% NaCl, P_{CO_2} = 1 bar (100 kPa), t = 20°C, 1,000 rpm, τ = 1.7 Pa, Re = 5,235, and St52 steel.*

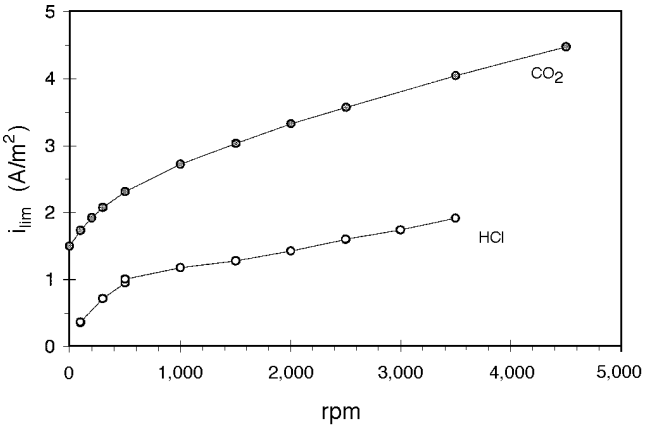

FIGURE 3. *Effect of CO_2 on i_{lim} obtained with a RCE, pH 4, water + 3% NaCl, P_{CO_2} = 1 bar (100 kPa), t = 20°C, and St52 steel.*

slopes of the H_2O and Fe^{2+} lines were ≈ 120 mV/decade and 40 mV/decade, respectively.

Figure 4 shows R_p measurements on St52 steel at different rotating speeds. The B values used to obtain the corrosion current (i_{corr}) were calculated by using the model presented below and typically were 16 mV to 20 mV. There was a flow effect on both corrosion curves which probably came from the mass-transfer i_{lim} for H^+ reduction. The effect of addition of CO_2 on the corrosion rate was small, as the reduction of H_2CO_3 gave a smaller contribution to the overall corrosion reaction than H^+ reduction at pH 4.

Measurements at pH 5 — Similar experiments were conducted at pH 5. In the solution with HCl at pH 5, there were few H^+ ions so that a distinct i_{lim} could not be observed (Figure 5). The dominant cathodic reaction was direct reduction of H_2O. Addition of CO_2 produced a clear increase in the overall cathodic current. The anodic line remained unchanged with a slope of ≈ 40 mV/decade.

The effect of CO_2 on i_{corr} at pH 5 was much stronger than at pH 4. The direct reduction of H_2CO_3 was the dominating cathodic reaction at pH 5. The contribution by the reduction of H^+ was much smaller than at pH 4. Over the whole range of rotation speeds at pH 5, i_{corr} was increased two to three times by addition of CO_2 (Figure 6). In this figure, the lines are nearly horizontal, indicating there was very little effect of flow. The reason for this was that the dominating cathodic reaction in CO_2 solutions was H_2CO_3 reduction, which was not flow sensitive. The same was true for the HCl solution at pH 5, where direct water reduction also was not flow sensitive.

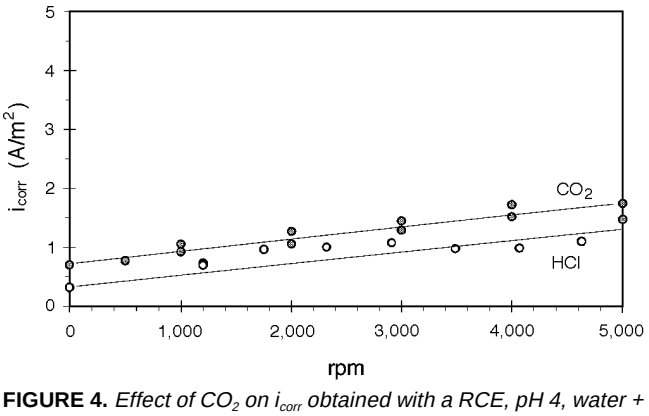

FIGURE 4. *Effect of CO_2 on i_{corr} obtained with a RCE, pH 4, water + 3% NaCl, P_{CO_2} = 1 bar (100 kPa), t = 20°C, and St52 steel.*

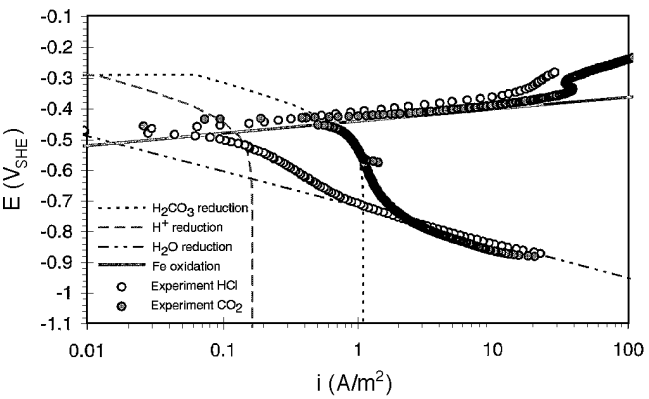

FIGURE 5. *CO_2 effect at pH 5, water + 3% NaCl, P_{CO_2} = 1 bar (100 kPa), t = 20°C, 1,000 rpm, τ = 1.7 Pa, Re = 5,235, and St52 steel.*

Effect of Velocity

Measurements at pH 3 Without CO_2 — In these experiments on St52 steel, the solution was purged with N_2, and pH was adjusted to 3 by adding HCl. Potentiodynamic sweeps for different rotational speeds are shown in Figure 7. Under these conditions, the main cathodic reaction was reduction of H^+ ions, as shown by Stern.[17] The observed flow-dependent cathodic i_{lim} represented the diffusion limit of H^+ ions from the bulk to the metal surface.[12,17] For higher overpotentials, the dominant cathodic reaction changes to the direct reduction of water, as shown by Stern.[17-18] Tafel behavior for the H^+ reduction reaction

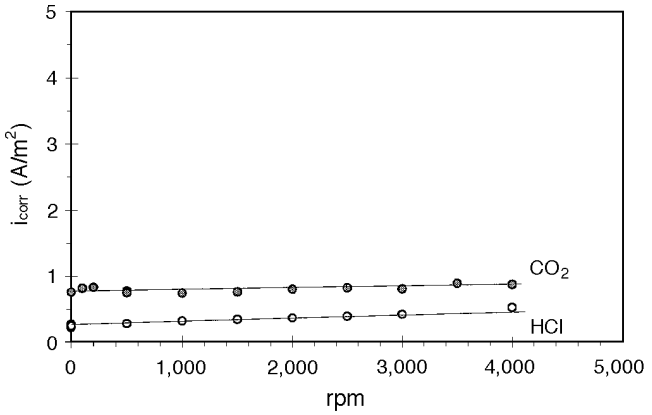

FIGURE 6. *Effect of CO_2 on i_{corr} obtained with a RCE, pH 5, water + 3% NaCl, P_{CO_2} = 1 bar (100 kPa), t = 20°C, and St52 steel.*

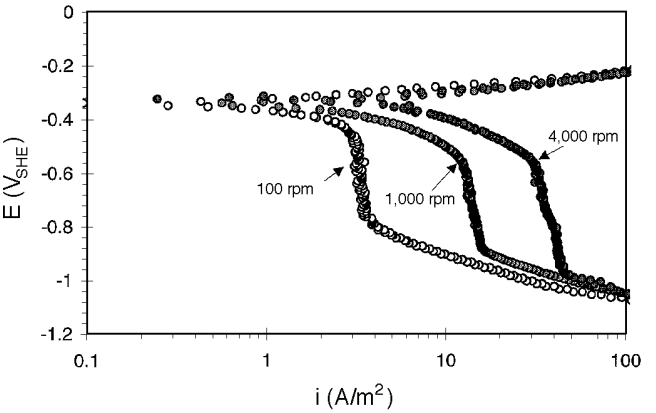

FIGURE 7. *Velocity effect in HCl solution at pH 3, water + 3% NaCl, P_{N_2} = 1 bar (100 kPa), t = 20°C, and St52 steel.*

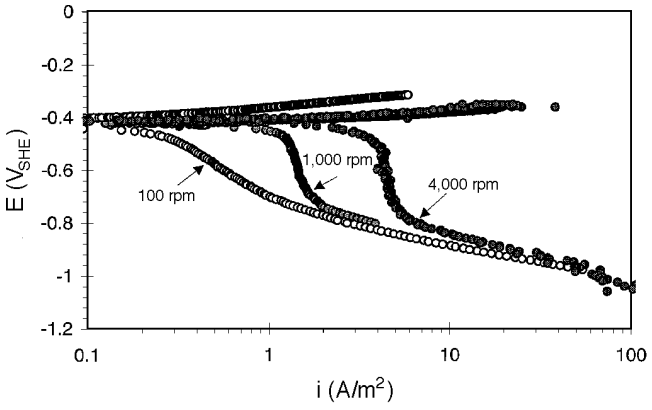

FIGURE 8. *Velocity effect in HCl solution at pH 4, water + 3% NaCl, P_{N_2} = 1 bar (100 kPa), t = 20°C, and St52 steel.*

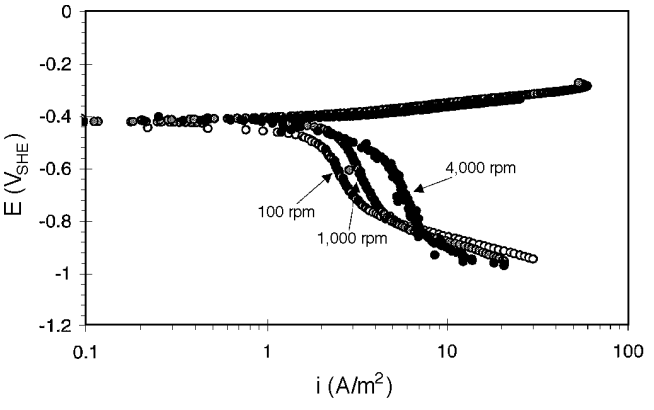

FIGURE 9. *Velocity effect in CO_2 solution at pH 4, water + 3% NaCl, P_{CO_2} = 1 bar (100 kPa), t = 20°C, and St52 steel.*

was clear only for the highest rotating speed, with a slope of ≈ 120 mV/decade. For higher overpotentials, all three cathodic curves converged onto the same line, which was the direct reduction of H_2O. The three anodic curves displayed clear Tafel behavior, with a slope of ≈ 40 mV/decade. No effect of rotating speed was noticed on the anodic reaction.

Measurements at pH 4 Without CO_2 — Potentiodynamic sweeps in a solution purged with N_2 at pH 4 (obtained by adding HCl) are shown in Figure 8 for St52 steel. The overall shape of the curves was similar to those in the experiments at pH 3 except that all i_{lim} values were 10 times lower. This was expected as the bulk concentration of H^+ ($[H^+]_b$) was 10 times lower at pH 4. For the lowest rotating speed (100 rpm), no i_{lim} was distinguishable as the dominating cathodic reaction throughout the measured range was the direct reduction of H_2O, which was under activation control.

Measurements at pH 4 with CO_2 — Subsequent experiments were conducted with the same steel in a solution purged with CO_2 instead of N_2. The pH was adjusted by adding $NaHCO_3$ (Figure 9). The potentiodynamic sweeps with CO_2 (Figure 9) had larger i_{lim} values when compared to HCl solutions (Figure 8) at the same pH. Further, the effect of rotation speed was much smaller, suggesting that there was a flow-insensitive component to i_{lim}. The i_{lim} value for the reduction of H_2CO_3 was chemical reaction-controlled and insensitive to flow. The flow sensitivity observed related to the contribution to i_{lim} by the reduction of H^+, which was mass transport-controlled. This could be seen by comparing i_{lim} at 1,000 rpm and 4,000 rpm with and without CO_2. In the CO_2 solution, the current increased by a factor of 1.8. In the solution without CO_2, the curent increased by a factor of 3.5. The anodic dissolution of iron was not affected by the flow.

Measurements at pH 5 with CO_2 — Flow sensitivity at pH 5 was tested for a solution purged with CO_2 where the pH was adjusted by adding $NaHCO_3$. A potentiodynamic sweep conducted on a St52 RCE at 1,000 rpm is presented in Figure 10 along with individual cathodic reactions and the theoretical sweep

generated using the model presented. The sweep was halted potentiostatically in the i_{lim} region, and the velocity (v) was changed from 1,000 rpm to 4,000 rpm and back. Cathodic i_{lim} values were mildly sensitive to flow (factor = 1.3). Pure diffusion control would have lead to a factor of 2.6 for a fourfold increase in the rotational speed for a rotating cylinder, where the rate of mass transfer was proportional to the speed raised to the power of 0.7, as given by the correlation of Eisenberg, et al.[19] Thus, the observed i_{lim} values were not controlled entirely by diffusion.

Since there were few H^+ ions in the solution at pH 5, the dominant cathodic reaction was H_2CO_3 reduction. As previously suggested, i_{lim} for this reaction was controlled by a slow hydration step, so no flow sensitivity was expected. The small change with rotation speed shown in Figure 10 could be attributed to the diffusion of present H^+ ions or H_2CO_3 molecules from the bulk to the surface.

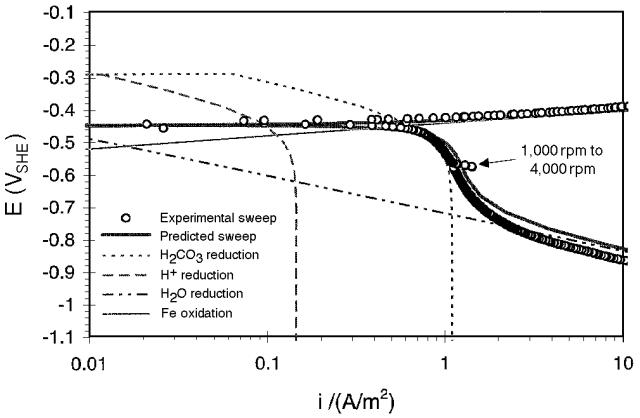

FIGURE 10. *Velocity effect in CO_2 solution at pH 5, water + 3% NaCl, P_{CO_2} = 1 bar (100 kPa), t = 20°C, and St52 steel.*

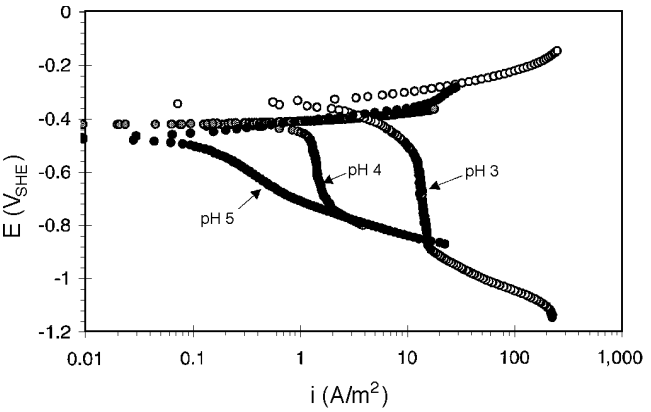

FIGURE 11. *pH effect in HCl solution, water + 3% NaCl, P_{N_2} = 1 bar (100 kPa), t = 20°C, 1,000 rpm, τ = 1.7 Pa, Re = 5,235, and St52 steel.*

Effect of pH

Solution Without CO_2 — The effect of pH is illustrated in Figure 11 for steel St52 in a solution purged with N_2 where the pH was adjusted by adding HCl. The i_{lim} values at 1,000 rpm were reduced proportionately to the H^+ concentration.

The position of the Tafel line for H_2O reduction stayed approximately the same over the whole pH range, with a slope of ≈ 120 mV/decade. This was in accordance with theory and agreed with the findings of Gray, et al.[13]

This analysis showed that the Tafel line for anodic dissolution of iron maintained the slope of 40 mV/decade over the whole pH range tested. The exchange current density changed according to:

$$\frac{\partial \log i_{0(Fe)}}{\partial pH} = 1 \qquad (1)$$

between pH 3 and 4, while it changed very little between pH 4 and 5, which was in agreement with findings of Bockris, et al.[20]

CO_2 Solution — With CO_2, the effect of changing the pH from 4 to 5 was to decrease i_{lim} by a factor of ≈ 3 (Figure 12). This was much less than expected for a tenfold decrease in H^+ concentration if the cathodic reaction was solely H^+ reduction. The reason for the threefold change was that the cathodic i_{lim} in CO_2 solutions was composed of a chemical reaction-limited component and a H^+-limiting component. The concentration of H_2CO_3 (and thus, the chemical reaction limited current) did not vary with pH, whereas i_{lim} for H^+ reduction was proportional to $[H^+]_b$. The relationship between pH and i_{lim} without CO_2 when the cathodic reaction was only H^+ reduction is shown in Figure 11, where a change in pH from 3 to 4 resulted in a decrease by a factor of 10 as was expected for a tenfold decrease in $[H^+]_b$. Comparisons of the effect of changing the pH between 4 and 5 for solutions with and without CO_2 were not possible as i_{lim} at pH 5 without CO_2 (Figure 11) was very small and indistinct.

Figure 12 shows pH had a small effect on the anodic dissolution reaction for St52 steel. A similar conclusion was reached previously by Videm.[21] The absence of a strong pH dependence of the anodic dissolution of iron in CO_2-containing environments was confirmed independently in another set of experiments with low-carbon X-65 pipeline steel (Figure 13). The measured anodic sweeps are shown along with individual electrochemical reactions and the theoretical sweep generated with the model. The pH had no clear effect on anodic dissolution of iron in CO_2 environments over the range of practical interest 4 < pH < 6 (pH values outside this range are less common for waters found in oil and gas production). In any case, the measured effect was far below the one seen previously in HCl solutions (Figure 11) and expected from the mechanism of Bockris.[20]

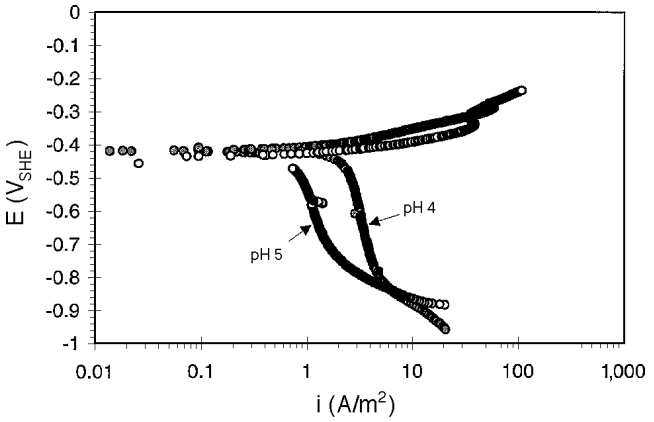

FIGURE 12. *pH effect in CO_2 solution, water + 3% NaCl, P_{CO_2} = 1 bar (100 kPa), t = 20°C, 1,000 rpm, τ = 1.7 Pa, Re = 5,235, and St52 steel.*

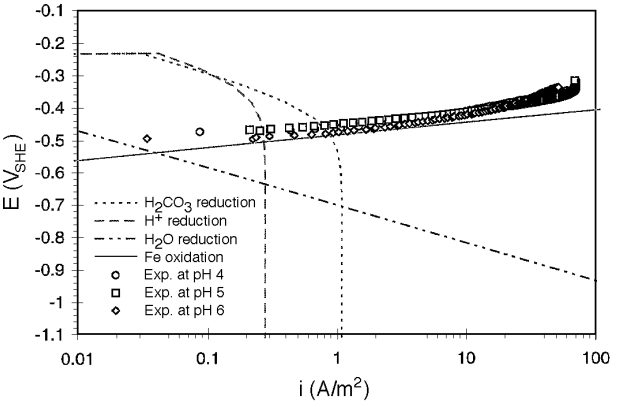

FIGURE 13. *pH effect on the iron dissolution reaction in CO_2 solution, water + 3% NaCl, P_{CO_2} = 1 bar (100 kPa), t = 20°C, and static using X-65 steel.*

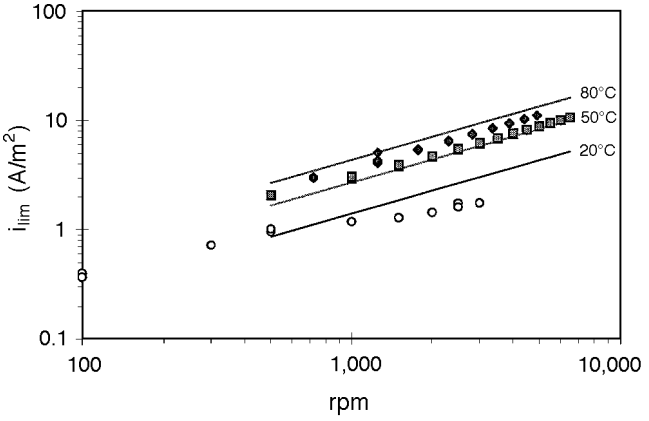

FIGURE 14. *Temperature effect on i_{lim} in HCl solution, pH 4, water + 1 % NaCl, P_{N_2} = 1 bar (100 kPa), obtained using a RCE.*

Effect of Temperature

Measurements at pH 4 Without CO_2 — Temperature was known to accelerate most of the chemical and electrochemical processes occurring in the present system. To distinguish the effect on individual reactions, experiments at higher temperatures were done first on X-65 steel in a solution purged with N_2 with pH adjusted by adding HCl.

The most pronounced effect was the increase in the mass transfer-controlled i_{lim} which resulted from an increase in the diffusion coefficient (D) for H^+ and a decrease in viscosity at higher temperatures. Measurements of the temperature dependence for i_{lim} were done at pH 4 using the RCE (Figure 14). At 20°C, the rotation speed was varied while the potential was held at –0.7 V_{SHE}, which was in the i_{lim} region. When results were compared with the correlation of Eisenberg, et al., for mass transfer to a rotating cylinder, the agreement was only partially satisfactory.[19] It was suspected that the reason was the shift of i_{lim} to lower potentials with increasing rotational speed (Figure 7), so that the performed potentiostatic measurements slightly underestimated the true i_{lim}. To correct this at higher temperatures (50°C and 80°C), a potentiodynamic sweep was done and then halted at a potential clearly in the i_{lim} region. The velocity then was changed from 1,000 rpm to 7,000 rpm and back. Agreement with the Eisenberg correlation was much better. This also indicated that measurement of the H^+ diffusion i_{lim} could be used in the future for quick characterization of the mass-transfer behavior of different hydrodynamic systems.

Measurements at pH 4 with CO_2 — Subsequent experiments were conducted where CO_2 was bubbled at different temperatures (20°C, 50°C, and 80°C) while maintaining the atmospheric pressure in the cells. However, because of the increasing water vapor pressure at 50°C and 80°C, the partial pressure of CO_2 (P_{CO_2}) in the cells was 0.88 bar (88 kPa) and 0.55 bar (55 kPa), respectively. Despite the lower P_{CO_2} at higher temperatures, the corrosion rate measured using R_p measurements increased from 1 mm/y (0.039 in./y) at 20°C to 2.5 mm/y (0.098 in./y) at 50°C and 3 mm/y (0.118 in./y) at 80°C. This was confirmed by looking at the potentiodynamic sweeps conducted at pH 5 on static specimen made from X-65 steel (Figure 15). The total cathodic reaction increased with increasing temperature. Since there were very few H^+ ions in the solution, the dominating cathodic reaction was probably H_2CO_3 reduction and direct H_2O reduction at high overpotentials.

Surprisingly, the anodic reaction shown on Figure 15 was not accelerated significantly at higher temperatures. Similar experiments were repeated many times without obtaining a consistent dependence of the anodic dissolution on temperature. In independent potentiostatic measurements, an Arrhenius-type temperature dependence was obtained for the anodic dissolution current of X-65

steel only for lower temperatures (20°C to 50°C). For higher temperatures, the rate of anodic dissolution of iron decreased, indicating a change in the rate-determining step or a different reaction mechanism. A more detailed study of this phenomenon will be conducted in the future.

PHYSICAL MODEL

The experimental findings led to a mechanistic model for CO_2 corrosion.

Cathodic Reactions

When CO_2 is added to an aqueous solution, it is hydrated to form a weak acid (H_2CO_3):

$$CO_2 + H_2O \leftrightarrow H_2CO_3 \quad (2)$$

Then, the H_2CO_3 is dissociated in two steps:

$$H_2CO_3 \leftrightarrow H^+ + HCO_3^- \quad (3)$$

$$HCO_3^- \leftrightarrow H^+ + CO_3^{2-} \quad (4)$$

The reduction of H^+:

$$H^+ + e^- \rightarrow H \quad (5)$$

is the most important cathodic reaction in an acidic solution. It has been shown previously[12,17] and confirmed in this project that, as the current density is increased, the resistance to the mass transfer of H^+, which causes a drop in the concentration at the metal surface, results in a deviation from Tafel behavior. Eventually, i_{lim} is attained. At higher pH values, the availability of H^+ decreases, and other competing cathodic reactions become important.

In CO_2 systems at low pH (< 4), H^+ reduction (Equation [5]) is still the dominant cathodic equation because of the high concentration of H^+. At intermediate pH (4 < pH < 6), which was the range of interest in this work, in addition to the H^+ reduction (Equation [5]), a new cathodic reaction becomes important, the direct reduction of H_2CO_3:

$$H_2CO_3 + e^- \rightarrow H + HCO_3^- \quad (6)$$

This additional cathodic reaction often is listed as the cause for the H_2CO_3 "to be more corrosive than a completely dissociated acid at the same pH."[11] The reaction has a limiting current that is controlled by a slow chemical step, the hydration of CO_2, as discussed in several other studies.[15-16] This i_{lim} is insensitive to flow. At currents above i_{lim} for H^+ or H_2CO_3 reduction, the dominant cathodic reaction changes to direct reduction of water:[18]

$$H_2O + e^- \rightarrow H + OH^- \quad (7)$$

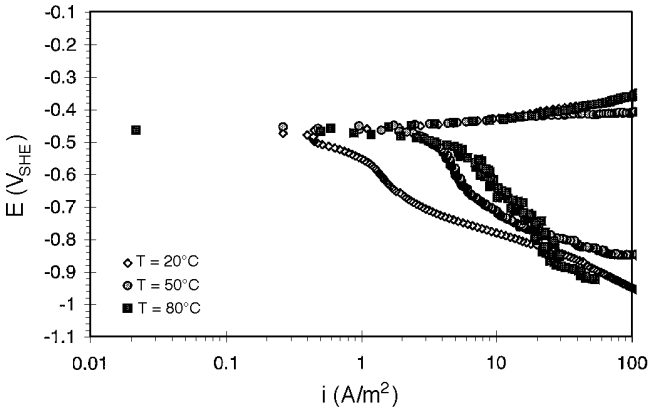

FIGURE 15. *Temperature effect in CO_2 solution, water + 1% NaCl, P_{CO_2} = 1 bar (100 kPa), pH 5, and static using X-65 steel.*

Anodic Reactions

In a water-CO_2 corroding system, it most often has been assumed that the sequence of anodic dissolution of iron is the same as it is in other acids,[11-12] as in the pH-dependent mechanism proposed by Bockris, et al.:[20]

$$Fe + OH^- \rightarrow FeOH + e^- \quad (8)$$

$$FeOH \xrightarrow{RD} FeOH^+ + e^- \quad (9)$$

$$FeOH^+ \rightarrow Fe^{2+} + OH^- \quad (10)$$

However, the present findings, in agreement with those of Videm,[21] did not support this assumption (> pH 4). It is difficult to propose a new mechanism for iron dissolution in CO_2-containing environments at this stage without a more detailed electrochemical study, but it was assumed that the iron dissolution reaction in CO_2-containing solutions proceeds with little influence of pH.

MATHEMATICAL MODEL

To build a predictive model of CO_2 corrosion, all of the previously described reactions must be quantified.

H^+ Reduction

For H^+ reduction, the cathodic part of the general rate equation, is used:[36]

$$i_{(H^+)} = i_{0(H^+)} \times \left\{ \frac{[H^+]_s}{[H^+]_b} \times \exp\left(-\frac{\alpha_c F}{RT} \eta \right) \right\} \quad (11)$$

Equation (11) takes into account the effect of resistance to charge transfer and mass transfer. The

surface concentration of H^+ ($[H^+]_s$) can be determined from the mass-transfer equation:

$$i_{(H^+)} = k_m F\left\{\left[H^+\right]_b - \left[H^+\right]_s\right\} \quad (12)$$

where k_m is the mass-transfer coefficient.

Solving Equations (11) and (12) for $[H^+]_s$ gives, after manipulation, the final current density-vs-voltage relationship for H^+ reduction:[22-23]

$$\frac{1}{i_{(H^+)}} = \frac{1}{i_{\alpha(H^+)}} + \frac{1}{i^d_{lim(H^+)}} \quad (13)$$

where $i^d_{lim(H^+)}$ is the diffusion limiting current density defined below (Equation [19]) and $i_{\alpha(H^+)}$ is the activation (charge transfer) current density in the absence of resistance to mass transfer:

$$i_{\alpha(H^+)} = i_{0(H^+)} \times 10^{-\frac{\eta}{b_c}} \quad (14)$$

Tafel Slope — The cathodic Tafel slope (b_c) for H^+ reduction appearing in Equation 14 is:

$$b_c = \frac{2.303RT}{\alpha_c F} \quad (15)$$

According to Bockris, et al.,[20] for H^+ reduction, $\alpha_c = 0.5$ giving $b_c = 0.118$ V at 25°C. This agreed well with the present findings.

Exchange Current Density — From the present experiments at the reference temperature (t_{ref}) = 20°C at pH 4, it was determined that the exchange current density for hydrogen ion reduction is $i^{ref}_{0(H^+)} \approx 5 \times 10^{-2}$ A/m^2. The pH dependence adopted from Bockris, et al.:[20]

$$\frac{\partial \log i_{0(H^+)}}{\partial pH} = -0.5 \quad (16)$$

agreed well with the experimental findings.

The temperature dependence of the exchange current density was modeled with an Arrhenius-type relation:

$$\frac{i_0}{i_0^{ref}} = e^{-\frac{\Delta H}{R}\left(\frac{1}{T} - \frac{1}{T_{ref}}\right)} \quad (17)$$

The enthalpy of activation for the H^+ reduction reaction was found to be $\Delta H_{(H^+)} \approx 30$ kJ/mol.

Reversible Potential — The reversible potential for H^+ reduction ($E_{rev[H+]}$) can be calculated as:

$$E_{rev(H^+)} = -\frac{2.303RT}{F} pH - \frac{2.303RT}{2F} \log P_{H_2} \quad (18)$$

where P_{H_2} is the partial pressure of hydrogen.

Limiting Current Density — The diffusion limiting component of the total current density appearing in Equation (13) is:

$$i^d_{lim(H^+)} = k_m F \times \left[H^+\right]_b \quad (19)$$

k_m in Equation (19) can be calculated from a correlation (e.g., straight pipe correlation of Berger and Hau):[24]

$$Sh = \frac{k_m l}{D} = 0.0165 \times Re^{0.86} \times Sc^{0.33} \quad (20)$$

or from a rotating cylinder correlation of Eisenberg, et al.:[19]

$$Sh = 0.0791 \times Re^{0.7} \times Sc^{0.356} \quad (21)$$

or any other correlation for the given flow geometry.

The temperature effect on D can be found from the Stokes-Einstein equation:

$$D = D_{ref} \times \frac{T}{T_{ref}} \times \frac{\mu_{ref}}{\mu} \quad (22)$$

For the reference temperature t_{ref} = 20°C, the dynamic viscosity of water is μ_{ref} = 1.002 kg/(m s),[25] and the diffusion coefficient for H^+ ions is $D_{ref(H+)} = 9.31 \times 10^{-9}$ m^2/s.[26]

Water density as a function of temperature was calculated as:[13]

$$\rho = 1{,}152.3 - 0.5116 \times T \quad (23)$$

and water viscosity:[25]

$$\mu = \mu_{ref} \times 10^{\frac{1.3272(20-t) - 0.001053(20-t)^2}{T+105}} \quad (24)$$

H_2CO_3 Reduction

It was suggested previously that H_2CO_3 reduction can be under activation control or under chemical reaction control for higher overvoltages. In a similar derivation to the one shown for H^+ reduction (Equations [11] through [13]), the current-vs-voltage relationship is obtained:

$$\frac{1}{i_{(H_2CO_3)}} = \frac{1}{i_{\alpha(H_2CO_3)}} + \frac{1}{i^r_{lim(H_2CO_3)}} \quad (25)$$

where $i^r_{lim(H_2CO_3)}$ is the chemical reaction limiting current density defined below (Equation [29]), and $i_{\alpha(H_2CO_3)}$ is the activation (charge transfer) current

density in the absence of chemical reaction resistance:

$$i_{\alpha(H_2CO_3)} = i_{0(H_2CO_3)} \times 10^{-\frac{\eta}{b_c}} \quad (26)$$

Tafel Slope — From the experiments, b_c for H_2CO_3 reduction in Equation (26) was found to be similar to that for H^+ reduction (≈ 120 mV/decade at 20°C), which was in agreement with deWaard and Milliams.[11]

Exchange Current Density — For t_{ref} = 20°C, the exchange current density for H_2CO_3 reduction in Equation (26) has a similar value as the one for H^+ reduction $i^{ref}_{o(H_2CO_3)} \approx 6 \times 10^{-2}$ A/m^2. Further, it can be shown that $i_{0(H_2CO_3)}$ is proportional to the H_2CO_3 concentration and the H^+ concentration:

$$i_{0(H_2CO_3)} \propto [H_2CO_3] \times [H^+]^{-0.5} \quad (27)$$

Thus, the pH dependence of the exchange current density is:

$$\frac{\partial \log i_{0(H_2CO_3)}}{\partial pH} = 0.5 \quad (28)$$

The temperature dependence of the exchange current density was modeled the same as for H^+ reduction according to Equation (17). The activation enthalpy for this reaction was found to be similar to the one for H^+ reduction $\Delta H_{(H_2CO_3)} \approx 30$ kJ/mol.

Reversible Potential — The two reactions, the reduction of H_2CO_3 and H^+, have the same reversible potential given by Equation (18).

Limiting Current Density — The CO_2 hydration reaction limiting current density $i^r_{lim(H_2CO_3)}$ can be obtained as:[27-28]

$$i^r_{lim(H_2CO_3)} = F \times [CO_2]_b \times \left(D_{H_2CO_3} K_{hyd} k^f_{hyd}\right)^{0.5} \quad (29)$$

This equation first was derived by Vetter and is strictly valid only for stagnant solutions.[27] When it was rederived from principles for flowing solutions, a similar expression was obtained but with a multiplier that accounted for the effect of flow. This multiplier is significantly different from unity only when the thickness of the mass-transfer boundary layer is of the same order of magnitude as the reaction layer. It is difficult to give a general rule when this is the case since it is affected by many factors. As a first approximation, it can be said that the Vetter's Equation (29) is correct at higher temperatures (T > 20°C) and low velocities (v ≤ 1 m/s [3.2 ft/s]) when the mass-transfer layer is much thicker than the reaction layer. Details on this correction will be published in the future.

The bulk concentration (b) of dissolved carbon dioxide ($[CO_2]_b$) can be obtained from P_{CO_2}:

$$[CO_2]_b = k^d_{CO_2} \times P_{CO_2} \quad (30)$$

The following equation was used to model the Henry's constant ($k^d_{CO_2}$) as a function of temperature:[29]

$$k^d_{CO_2} = 0.0454\left(1.6616 - 5.736 \times 10^{-2} t + 1.031 \times 10^{-3} t^2 - 9.68 \times 10^{-6} t^3 + 4.471 \times 10^{-8} t^4 - 7.912 \times 10^{-11} t^5\right) \quad (31)$$

The diffusion coefficient for H_2CO_3 in water ($D_{H_2CO_3}$) is calculated from a reference value (1.3 x 10^{-9} m^2/s at 25°C)[12,28] and the Stokes-Einstein Equation (22). The equilibrium constant for the CO_2 hydration reaction is K_{hyd} = 2.58 x 10^{-3} and does not change with temperature in the domain of interest.[31]

The forward reaction rate for the CO_2 hydration reaction (K^f_{hyd}) is a function of temperature.[30-31] An attempt was made to use the equation proposed by Stachewski,[30] but low values for the hydration rate were obtained for higher temperatures (50°C and 80°C). A more detailed search showed that rather large variations on the value of k^f_{hyd} at high temperatures exist in the literature. Therefore, keeping the same form of the equation, new coefficients were determined that gave a much better agreement with the flow-independent, chemical reaction rate-controlled limiting currents measured in CO_2 solutions at higher temperatures.

$$k^f_{hyd} = 10^{169.2 - 53.0 \log T - \frac{11{,}715}{T}} \quad (32)$$

Water Reduction

Since water molecules are present in unlimited quantities at the metal surface, it can be assumed that the reduction rate of H_2O is controlled by the charge-transfer process and, hence, pure Tafel behavior:

$$i_{(H_2O)} = i_{0(H_2O)} \times 10^{-\frac{\eta}{b_c}} \quad (33)$$

Since the reduction of H_2O and H^+ are equivalent thermodynamically, in the sense that they have the same E_{rev} at a given pH, E_{rev} for reduction of H_2O is given by the same Equation (18) as for H^+ reduction.[12,34] From the experiments at t_{ref} = 20°C, it was determined that the exchange current density for

H_2O reduction is $i_{0(H_2O)} \approx 3 \times 10^{-5}$ A/m^2. No systematic dependence of the exchange current density for this reaction was found for 3 < pH < 6. The temperature sensitivity was modeled according to Equation (17), and a similar activation enthalpy was found as for the previous two reactions: $\Delta H_{(H_2O)} \approx 30$ kJ/mol. The Tafel slope for H_2O reduction was found to be the same as that for H^+ reduction (≈ 120 mV/decade at 20°C).

Oxygen Reduction

Oxygen reduction was included in the model to enable estimation of the effect of any oxygen presence in CO_2 systems (laboratory or field) on the corrosion rate. Since E_{rev} for oxygen reduction is much higher than for the other mentioned reactions, pure mass-transfer control can be assumed for this reaction in the electrode potential region of interest. The diffusion limiting current density for oxygen reduction, $O_2 + 4H^+ + 4e = 2H_2O$, is:

$$i^d_{lim(O_2)} = 4k_m F \times \left[O_2\right]_b \qquad (34)$$

k_m can be determined from a correlation relating the Sherwood, Reynolds, and Schmidt numbers, as shown above for H^+ reduction. For t_{ref} = 20°C, the diffusion coefficient for O_2 is $D_{ref(O_2)} = 2.09 \times 10^{-9}$ m^2/s.[26]

Anodic Dissolution of Iron

In the present experiments, the corrosion of two low-carbon steels was studied. For both steels, the anodic dissolution of iron at the corrosion potential (and up to 200 mV above) was under activation control. Thus, pure Tafel behavior can be assumed close to the corrosion potential:

$$i_{(Fe)} = i_{0(Fe)} \times 10^{\frac{\eta}{b_a}} \qquad (35)$$

Tafel Slope — The anodic Tafel slope (b_a) for anodic iron dissolution is:

$$b_a = \frac{2.303RT}{\alpha_a F} \qquad (36)$$

According to Bockris, et al.,[20] α_a = 1.5 giving b_a = 40 mV at 25°C, which agreed very well with the experimental findings.

Exchange Current Density — The concentration of ferrous ions in solution does not affect the dissolution kinetics of iron in the absence of film formation.[32,35] The Tafel line for the anodic dissolution is not affected by the rise in the concentration of ferrous ions required for their transport away from the anode.[32] To construct the anodic dissolution polarization line for iron, the exchange current density is required along with b_a.

As shown by West, the relationship between E_{rev} and i_0 for the anodic dissolution of a metal is:[36]

$$E_{rev} - E^1_{rev} = b \log \frac{i_0}{i^1_0} \qquad (37)$$

Thus, if the value of i_0 is known at any concentration of ferrous ions, from experimental data for a given electrolyte, the Tafel line can be plotted which will apply regardless of the concentration of ferrous ions in solution.

In the present experiments, no dependence of the iron dissolution rate on Fe^{2+} concentration was found, in agreement with the above. This finding was used in the model to construct the curve for Fe^{2+} dissolution. Since it was shown experimentally that the anodic line for both steels was not affected significantly by pH over the pH range 4 to 6, it was sufficient to extract from the experiments the $i_{0(Fe)}$ value for one reference potential, and the anodic dissolution line was defined.

The activation enthalpy for this reaction was found to be $\Delta H_{(Fe^{2+})} \approx 40$ kJ/mol for lower temperatures (20°C to 50°C). As previously mentioned, at higher temperatures (> 50°C) this trend was reversed, so no firm conclusion on the effect of temperature on iron dissolution could be reached at the present stage.

The steel type had the largest effect on anodic dissolution. Very different $i_{0(Fe)}$ values were found for the two steels tested (Figure 16). At a reference potential E_{rev} = –0.488 V in the case of the St52 steel, the exchange current density was found to be $i_{0(Fe)} \approx 0.1$ A/m^2, while for the X-65 steel, it was an order of magnitude higher at $i_{0(Fe)} \approx 1$ A/m^2. Such variations in the values of i_0 between different steels was not unexpected.

IMPLEMENTATION OF THE MODEL

The present electrochemical model was implemented in Microsoft Excel 5.0 for Windows† to exploit the user friendly interface and the advanced graphical capabilities. The built-in equation solver is somewhat slow, so use of other programming languages can be beneficial.

The model requires as input: temperature, pH, P_{CO_2}, oxygen concentration, type of steel, and the flow geometry. Pipe flow or a rotating cylinder flow can be selected. For pipe flow, the inputs are water velocity and pipe diameter, while for rotating cylinder flow, the inputs are the rotating speed and cylinder diameter.

Once the input parameters are determined, the program generates an updated graph with the individual and total cathodic and anodic curves. The intersection of the total cathodic curve with the

anodic curve gives the corrosion potential (E_{corr}) by solving:

$$i_{(H^+)} + i_{(H_2CO_3)} + i_{(H_2O)} + i_{(O_2)} = i_{(Fe)} \quad (38)$$

i_{corr} is calculated from the anodic curve Equation (35) and the known E_{corr}. It is possible to display the theoretical polarization curve (sweep) generated by Equation (38) or, by using the same equation, the theoretical E-vs-i curve for small overpotentials often used to determine R_p can be displayed. The slope dE/di at the corrosion potential can be calculated by numerically differentiating Equation (38). This information can be used for calculating the theoretical B value since i_{corr} is known:

$$B = \left(\frac{dE}{di}\right)_{E_{corr}} \times i_{corr} \quad (39)$$

The model enables numerous other possibilities including: combinations of individual and total polarization curves, overlaying theoretical and experimental sweeps, and R_p plots.

MODEL VALIDATION

Performance of the model was validated by comparing the predictions with results from independent glass loop experiments. Experimental data were obtained for flow through a straight pipe, d_{pipe} = 15 mm (0.59 in.) at v = 2 m/s (6.56 ft/s) and P_{CO_2} = 1 bar (100 kPa) with no protective films present. A more detailed description of these experiments has been given elsewhere.[33] Comparisons for t = 20°C, 50°C, and 80°C and pH 4, 5, and 6 are shown in Figure 17. Reasonably good agreement was obtained over the whole range. In some experiments (which typically lasted a few days), the corrosion rate varied as films formed at higher temperatures.[33]

Subsequently, predictions made with the present model were compared with the experimentally based models of deWaard and Lotz[1] and with the model of Dugstad, et al.[2] The latter two models are semi-empirical, and each is calibrated with a different set of experimental data with somewhat different steels. Predictions with the present model were made by using $i_{0(Fe)}$ = 0.1 A/m^2 determined for the St52 steel used in the present experiments.

pH Effect

The predictions of the pH effect on the CO_2 corrosion were made for the case of a solution saturated with 1 bar (100 kPa) CO_2, t = 20°C, v = 1 m/s (3.2 ft/s), d_{pipe} = 25 mm (0.98 in.) giving Re = 25,000. A comparison of the predictions made with different models is presented in Figure 18. The present predictions were somewhere in between the predictions

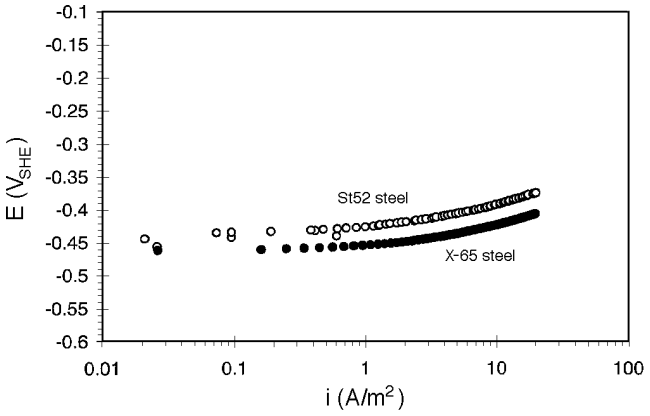

FIGURE 16. *Comparison of the anodic dissolution lines for the X-65 and St52 steels in CO_2 solution, water + 1 % NaCl, t = 20°C, P_{CO_2} = 1 bar (100 kPa), pH 5, and static.*

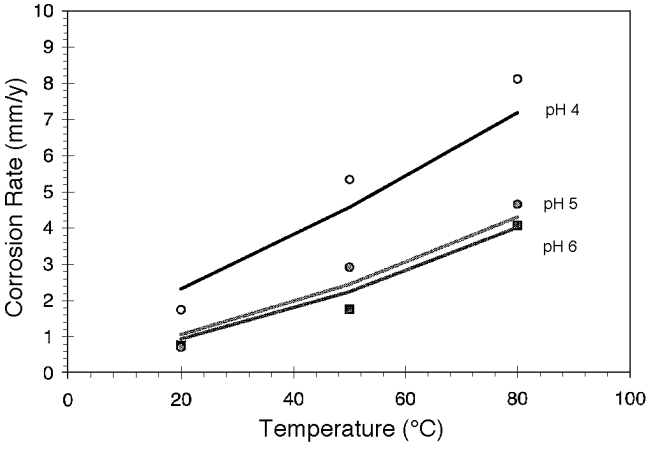

FIGURE 17. *Comparison of the model predictions with results from independent glass loop experiments with X-65 steel in water + 1 % NaCl at v = 2 m/s (6.56 ft/s), τ = 12 Pa, P_{CO_2} = 1 bar (100 kPa), and Re = 30,000.*

made with the models of deWaard and Lotz and Dugstad, et al., except at pH < 3.5. In this range, the H^+ reduction becomes the dominant reaction as previously shown. The models of deWaard and Lotz and Dugstad, et al., are not valid in this domain.

Effect of Flow Rate

A comparison of the flow effect predictions made with different models is presented in Figure 19 for pH 4, t = 20°C, P_{CO_2} = 1 bar (100 kPa). Agreement of the present model with the deWaard and Lotz model was nearly complete except at very low velocities. This was a result of the velocity corrections implemented in the latest version of the deWaard and Lotz model, through the so-called "resistance model," which resembles in form the present Equations (13) and (25). However, the deWaard and Lotz model lacks the physical background presented here, which is com-

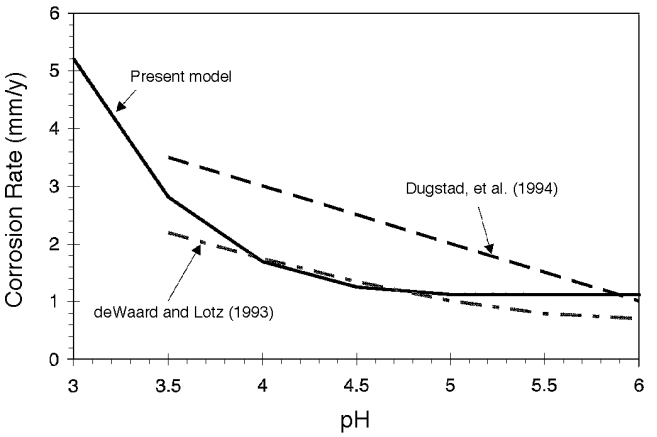

FIGURE 18. *Comparison of predicted pH effect on the corrosion rate for the case of a solution saturated with P_{CO_2} = 1 bar (100 kPa), t = 20°C, v = 1 m/s (3.2 ft/s), τ = 3.1 Pa, d_{pipe} = 25 mm (0.98 in.), and Re = 25,000.*

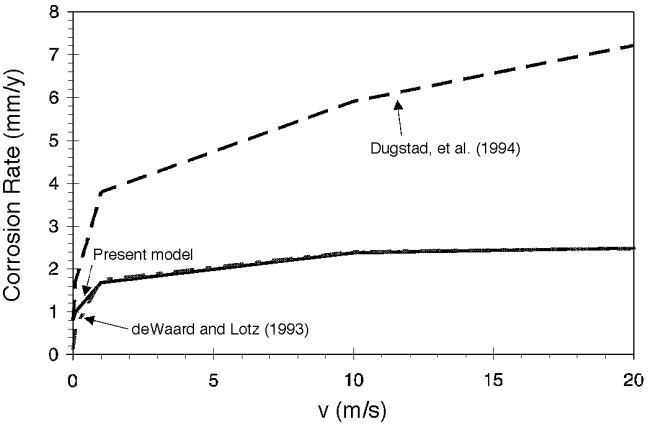

FIGURE 19. *Comparison of predicted velocity effects on the corrosion rate for the case of a solution saturated with P_{CO_2} = 1 bar (100 kPa), pH 4, t = 20°C, and d_{pipe} = 25 mm (0.98 in.).*

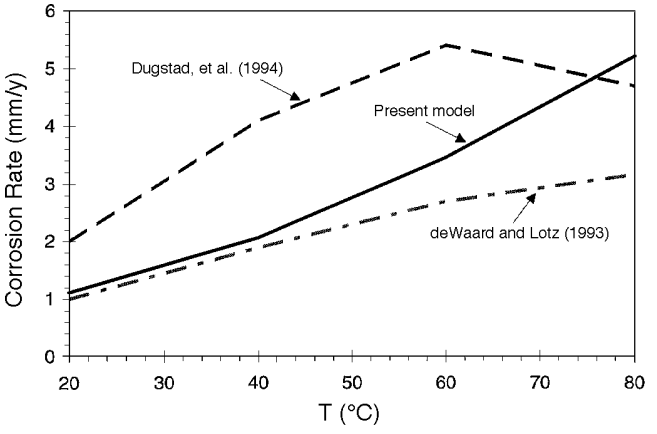

FIGURE 20. *Comparison of predicted temperature effects on the corrosion rate for the case of a solution saturated with P_{CO_2} = 1 bar (100 kPa), v = 1 m/s (3.2 ft/s), τ = 3.1 Pa, pH 5, d_{pipe} = 25 mm (0.98 in.), and Re = 25,000.*

pensated by a calibration constant in their resistance model. The Dugstad, et al., model showed a similar flow dependence as the other two models, but at a higher level. It was shown later that the reason is probably that different steels were used in different studies. It was demonstrated in the present study that very different rates of anodic dissolution were obtained with apparently not-so-different steels. With a choice of a different $i_{0(Fe)}$ in the present model that corresponded better to the steel used in the study of Dugstad, et al., a much better agreement between the two models could be achieved.

Effect of Temperature

The predicted temperature dependence of the corrosion rate made with the present model is compared with the predictions of the other two models in Figure 20 for pH 5, v = 1 m/s (3.2 ft/s), P_{CO_2} = 1 bar (100 kPa). From 20°C to 40°C, predictions of the present model were close to the predictions of the deWaard and Lotz model. For temperatures > 40°C, the discrepancy increased. The Dugstad, et al., model predicted higher corrosion rates than other two models. The temperature dependence curve produced with the Dugstad model had a different character as it included a decrease of the corrosion rates at higher temperatures due to protective film formation. The same correction factor present in the deWaard and Lotz model was responsible for the difference between the present predictions and the deWaard and Lotz model at higher temperatures.

Effect of P_{CO_2}

The effect of P_{CO_2} is demonstrated by comparing the three models for pH 4, t = 20°C, v = 1 m/s (3.2 ft/s). All three models have a similar power law dependence between 1 bar (100 kPa) and 10 bar (1,000 kPa) CO_2 with the exponent close to 0.7 (Figure 21). The main difference is at P_{CO_2} < 1 bar (100 kPa), where the present model did not predict any correlation (because H^+ reduction dominated) while the models of deWaard and Lotz and Dugstad, et al., extrapolated the same power law dependence into this region. It was interesting that the present model reproduced the experimentally observed 0.7 power law dependence directly from the fundamental electrokinetic equations.

CONCLUSIONS

❖ In the HCl solutions purged with N_2 at pH 3 and 4, the dominant cathodic reaction was H^+ reduction except at very low rotation speeds and static conditions, when it changed to H_2O reduction. Tafel

behavior for H^+ reduction could be observed only at high rotation speed (slope 120 mV/decade). Diffusion limiting currents were observed and could be predicted by using mass-transfer correlations such as the correlation of Eisenberg, et al.,[19] for a rotating cylinder. At currents beyond the limiting current and especially for pH 5 and higher, direct reduction of H_2O became the dominant cathodic reaction, which was under activation control (slope 120 mV/decade). Anodic dissolution of iron followed Tafel behavior for small overpotentials (slope 40 mV/decade) and was not flow sensitive. The pH dependence agreed well with the mechanism of Bockris, et al.,[20] up to pH 4. The corrosion rate at 20°C and pH 4 was under mixed control (activation-diffusion) and was flow sensitive. For high rotation speeds, it became activation controlled. At pH 5, the corrosion rate was controlled by direct reduction of H_2O and was not flow sensitive.

❖ In CO_2 solutions, it was confirmed that there was an additional cathodic reaction: direct reduction of H_2CO_3. At pH 4, both H^+ and H_2CO_3 reduction were of similar magnitude at low rotation speeds. For higher rotation speeds, reduction of H^+ dominated. At pH 5, reduction of H_2CO_3 was the dominant cathodic reaction. Limiting currents for this reaction were found to be under chemical reaction-control and nearly flow insensitive. Reduction of H_2O was not affected by the presence of CO_2. This reaction was under activation control and was not flow or pH sensitive. The pH had very little effect on anodic dissolution of iron in CO_2 environments over the range of practical interest $4 < pH < 6$. i_{corr} at 20°C and pH 4 was under mixed control (activation-diffusion chemical reaction) and flow sensitive. At pH 5, i_{corr} was under mixed control (activation-chemical reaction) and flow insensitive.

❖ The model of electrochemical reactions occurring in a water-CO_2 system takes into account the following cathodic reactions: H^+ reduction, H_2CO_3 reduction, direct water reduction, and oxygen reduction. One anodic reaction was accounted for: iron dissolution. The data generated by the model can be used to:

— Predict the corrosion rate;

— Determine the governing corrosion mechanism (activation, diffusion, reaction, or mixed control);

— Conduct sensitivity tests with respect to the input parameters of temperature, pH, velocity, and P_{CO_2};

— Help understand and explain data from electrochemical measurements such as potentiodynamic sweeps and R_p measurements; and

— Obtain the theoretical B value in the case of multiple cathodic reactions.

Performance of the model was validated by comparing the predictions with results from independent loop experiments. Good agreement was obtained for t = 20°C, 50°C, and 80°C and pH 4, 5, and 6.

❖ Predictions made with the present model were compared with performance of the other best-known

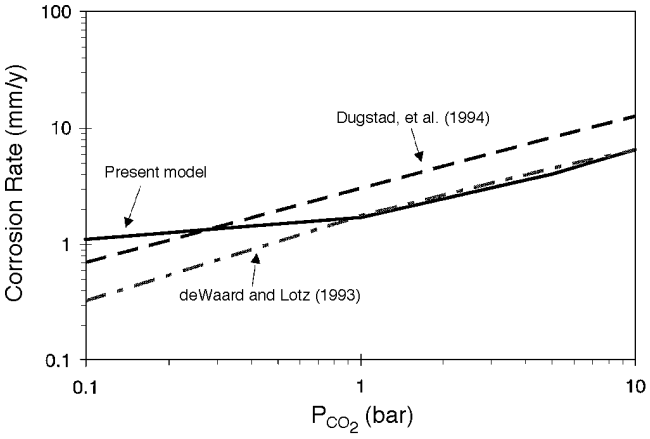

FIGURE 21. *Comparison of predicted P_{CO_2} effect on the corrosion rate for the case of a solution at pH 4, t = 20°C, v = 1 m/s (3.2 ft/s), τ = 3.1 Pa, d_{pipe} = 25 mm (0.98 in.), and Re = 25,000.*

CO_2 corrosion prediction models. The present model performed similarly to the latest version of the model of deWaard and Lotz. This was not surprising since the main operating assumption of the original deWaard and Milliams model, charge-transfer controlled H_2CO_3 reduction, also is included in the present model. The so-called "resistance model" built into the latest deWaard and Lotz model resembles in form some of the present theoretical equations. The predictions presented here were quite different from the ones made with the empirical model of Dugstad, et al.[2] Some latest simulations have shown that their results also can be simulated by selecting the anodic exchange current density appropriate for the steel used in their experiments, which was unknown previously.

❖ Compared to all previous models, the present theoretical model gives a much clearer picture of the corrosion mechanisms and of the effect of key parameters. Most of the important constants in the present model, which were determined experimentally, are physically meaningful. Being theoretical, the model is open for inclusion of new concepts such as a more detailed treatment of the transport process, which could lead to predictions of protective film formation or inclusion of an inhibitor effect in a physically correct way.

ACKNOWLEDGMENTS

This work was supported financially by Statoil and the Norwegian Council for Scientific Research.

NOMENCLATURE

b_a, b_c	anodic and cathodic Tafel slope (V/decade)
$[CO_2]_b$	bulk concentration of dissolved carbon dioxide (mol/m^3)

D	diffusion coefficient (m^2/s)
E_{rev}	reversible potential (V)
F	Faraday constant (96,490 coul/equiv.)
$[H^+]_s$, $[H^+]_b$	surface and bulk H^+ concentration (mol/m^3)
i	current density (A/m^2)
i_a	activation component of the total current density (A/m^2)
i_0	exchange current density (A/m^2)
i^d_{lim}	diffusion limiting current density (A/m^2)
i^r_{lim}	chemical reaction limiting current density (A/m^2)
k_m	mass-transfer coefficient (m/s)
k^f_{hyd}	forward reaction rate for the CO_2 hydration reaction (l/s)
$k^d_{CO_2}$	Henry's constant, ($mol/[m^3$ bar])
K_{hyd}	equilibrium constant for the CO_2 hydration reaction
l	characteristic length, pipe or cylinder diameter (m)
$[O_2]_b$	bulk concentration of oxygen (mol/m^3)
P_{CO_2}	partial pressure of CO_2 gas (bar)
P_{H_2}	partial pressure of hydrogen gas, bar
R	universal gas constant (8.3143 J/(mol K)
$Re = \rho v l/\mu$	Reynolds number
$Sc = \mu/\rho D$	Schmidt number
$Sh = k_m l/D$	Sherwood number
t	temperature (°C)
T	absolute temperature (K)
v	velocity (m/s)
α_c, α_a	apparent transfer coefficients
ΔH	enthalpy of activation (J/mol)
$\eta = E - E_{rev}$	overpotential (V)
μ	viscosity (kg/m-s)
ρ	density (kg/m^3)

REFERENCES

1. C. deWaard, U. Lotz, "Prediction of CO_2 Corrosion of Carbon Steel," CORROSION/93, paper no. 69 (Houston, TX: NACE, 1993).
2. A. Dugstad, L. Lunde, K. Videm, "Parametric Study of CO_2 Corrosion of Carbon Steel," CORROSION/94, paper no. 14 (Houston, TX: NACE, 1994).
3. E.L. Pye, M.L. Pye, F.H. Brock, "Pol-Plot: Basic Electrode Software, Simple to Complex," CORROSION/88, paper no. 102 (Houston, TX: NACE, 1988).
4. G. Rochini, "Extension of the Stern and Geary's Method for Calculating of Electrochemical Parameters with Inter1 Code," CORROSION/88, paper no. 103 (Houston, TX: NACE, 1988).
5. G. Rochini, "Determination of the Validity Interval of Linear Approximation Method with Inter1 Code," CORROSION/88, paper no. 105 (Houston, TX: NACE, 1988).
6. J.G. Hines, Brit. Corros. J. 18 (1983): p. 10.
7. F. Mansfeld, Corrosion 29 (1983): p. 397.
8. K.R. Trethewey, J.S. Keenan, "Microcomputer-Based Corrosion Modeling Applied to Polarization Curves," in Computer Modelling in Corrosion, ed. R.S. Munn, ASTM STP 1,154 (West Conshohocken, PA: ASTM, 1992), p. 113.
9. J.M. Costa, M. Vilarassa, "Microcomputer Programs for Corrosion Education," in Proc. U.K. Corrosion'88, vol. 3 (1988): p. 99.
10. M.R. Bonis, J.L. Crolet, "Basics of the Prediction of the Risks of CO_2 Corrosion in Oil and Gas Wells," CORROSION/89, paper no. 466 (Houston, TX: NACE, 1989).
11. C. deWaard, D.E. Milliams, Corrosion 31 (1975): p. 131.
12. L.G.S. Gray, B.G. Anderson, M.J. Danysh, P.G. Tremaine, "Mechanism of Carbon Steel Corrosion in Brines Containing Dissolved Carbon Dioxide at pH 4," CORROSION/89, paper no. 464 (Houston, TX: NACE, 1989).
13. L.G.S. Gray, B.G. Anderson, M.J. Danysh, P.R. Tremaine, "Effect of pH and Temperature on the Mechanism of Carbon Steel Corrosion by Aqueous Carbon Dioxide," CORROSION/90, paper no. 40 (Houston, TX: NACE, 1990).
14. S. Nesic, "Prediction of Transport Processes in CO_2 Corrosion," Progress in the Understanding and Prevention of Corrosion, Proc. 10th Europ. Corros. Cong., vol. 1 (London, England: Institute of Metals, 1993), p. 539.
15. G. Schmitt, B. Rothman, Werkst. Korros. 28 (1977): p. 816.
16. E. Eriksrud, T. Søntvedt, "Effect of Flow on CO_2 Corrosion Rates in Real and Synthetic Formation Waters," in Advances in CO_2 Corrosion, vol. 1. Proc. CORROSION/83 Symp. CO_2 Corrosion in the Oil and Gas Industry, eds. R.H. Hausler, H.P. Goddard (Houston, TX: NACE, 1984), p. 20.
17. M. Stern, J. Electrochem. Soc. 102 (1955): p. 609.
18. P. Delahay, J. Amer. Chem. Soc. 74 (1952): p. 3,497.
19. M. Eisenberg, C.W. Tobias, C.R. Wilke, J. Electrochem. Soc. 101 (1954): p. 306.
20. J.O'M. Bockris, D. Drazic, A.R. Despic, Electrochim. Acta 4 (1961): p. 325.
21. K. Videm, "Fundamental Studies aimed at Improving Models for Prediction of CO_2 Corrosion," in Progress in the Understanding and Prevention of Corrosion, Proc. 10th Europ. Corros. Cong., vol. 1 (London, England: Institute of Metals, 1993), p. 513.
22. V.S. Bagotzky, Fundamentals of Electrochemistry (New York, NY: Plenum Press, 1993), p. 141.
23. A.J. Bard, L.R. Faulkner, "Electrochemical Methods (New York, NY: John Wiley and Sons, 1980), p. 110.
24. F.P. Berger, K.-F. F.-L Hau, Int. J. Heat Mass Trans. 20 (1977): p. 1,185.
25. Handbook of Chemistry and Physics, 66th ed. (Boca Raton, Fl: CRC Press Inc., 1985), p. F-37.
26. P.W. Atkins, Physical Chemistry, 2nd ed. (Oxford, England: Oxford University Press, 1982), p. 905.
27. K.J. Vetter, Electrochemical Kinetics, Theoretical Aspects, Sections 1, 2, and 3 of Electrochemical Kinetics: Theoretical and Experimental Aspects (translation from German) (New York, NY: Academic Press, 1967), p. 235.
28. T. Hurlen, S. Gunvaldsen, R. Tunold, F. Blaker, P.G. Lunde, J. Electroanal. Chem. 180 (1984): p. 511.
29. IUPAC, Chemical Data Series, No. 21, "Stability Constants for Metal Ion Complexes, Part A: Inorganic Ligands" (Elmsford, NY: Pergamon Press, 1982).
30. D. Stachewski, Chemie-Ing.-Techn. 41 (1969): p. 1,111.
31. D.A. Palmer, R.V. Eldik, Chem. Rev. 83 (1983): p. 651.
32. J. Postlethwaite, Electrochim. Acta 15 (1970): p. 1,847.
33. S. Nesic, G.T. Solvi, J. Enerhaug, "Comparison of the Rotating Cylinder and Pipe Flow Tests for Flow Sensitive CO_2 Corrosion," CORROSION/95, paper no. 130 (Houston, TX: NACE, 1995).
34. H. Kaesche, Metallic Corrosion (Houston, TX: NACE, 1985), p. 113.
35. W. Lorenz, K. Heusler, "Anodic Dissolution of Iron Group Metals," in Corrosion Mechanisms, ed. F. Mansfeld (New York, NY: Marcel Dekker, 1987).
36. J.M. West, Electrodeposition and Corrosion Processes (Van Nostrand, 1964), p. 36.